

Antibacterial and biodegradable tissue nano-adhesives for rapid wound closure

Meng-meng Lu,^{1,2} Jing Bai,³
Dan Shao,^{4,5} Jing Qiu,^{1,2}
Ming Li,^{1,2} Xiao Zheng,⁵
Yun Xiao,⁶ Zheng Wang,⁴
Zhi-min Chang,⁴ Li Chen,⁵
Wen-fei Dong,⁴ Chun-bo
Tang^{1,2}

¹Department of Oral Implantology, Affiliated Hospital of Stomatology, Nanjing Medical University, Nanjing, 210029, China; ²Jiangsu Key Laboratory of Oral Diseases, Nanjing Medical University, Nanjing, 210029, China; ³School of Materials Science and Engineering, Southeast University, Jiangsu Key Laboratory for Advanced Metallic Materials, Jiangning, Nanjing 211189, Jiangsu, China; ⁴CAS Key Laboratory of Bio Medical Diagnostics, Suzhou Institute of Biomedical Engineering and Technology, Chinese Academy of Sciences, Suzhou 215163, China; ⁵Department of Pharmacology, College of Basic Medical Sciences, School of Nursing, Jilin University, Changchun 130021, China; ⁶National Engineering Research Center for Biomaterials, Sichuan University, Chengdu, 610064, China

Correspondence: Chun-bo Tang
Jiangsu Key Laboratory of Oral Diseases,
Nanjing Medical University; Department
of Oral Implantology, Affiliated Hospital
of Stomatology, Nanjing Medical
University, Nanjing 210029, China
Tel +86 258 503 1834
Email cbtang@njmu.edu.cn

Dan Shao
CAS Key Laboratory of Bio Medical
Diagnostics, Suzhou Institute of
Biomedical Engineering and Technology,
Chinese Academy of Sciences, 88 Keling
RD, Suzhou, Jiangsu 215163, China
Tel +86 512 6958 8307
Email stanauagate@outlook.com

Background: Although various organic tissue adhesives designed to facilitate wound healing are gaining popularity in diverse clinical applications, they present significant inherent limitations, such as rejection, infections, toxicity and/or excessive swelling. It is highly desirable to develop efficient, biocompatible and anti-bacterial tissue adhesives for skin wound healing.

Purpose: Inspired by the fact that inorganic nanoparticles can directly glue tissues through the “nanobridging effect”, herein disulfide bond-bridged nanosilver-decorated mesoporous silica nanoparticles (Ag-MSNs) was constructed as an effective and safe tissue adhesive with antibacterial and degradable properties for wound closure and healing.

Materials and methods: Ag-MSNs was fabricated by controlled reduce of ultrasmall nanosilvers onto the both surface and large pore of biodegradable MSNs. The obtained MSNs were characterized by transmission electron microscopy, Fourier transform infrared spectroscopy, energy-dispersive X-ray spectroscopy, and measurement of size distribution, zeta potential, and mesopore properties. Furthermore, adhesion strength test, anti-bacterial assessment, mouse skin wound model, and MTT assays were used to investigate the tissue adhesive property, anti-bacterial effect, biodegradability and biocompatibility of the Ag-MSNs.

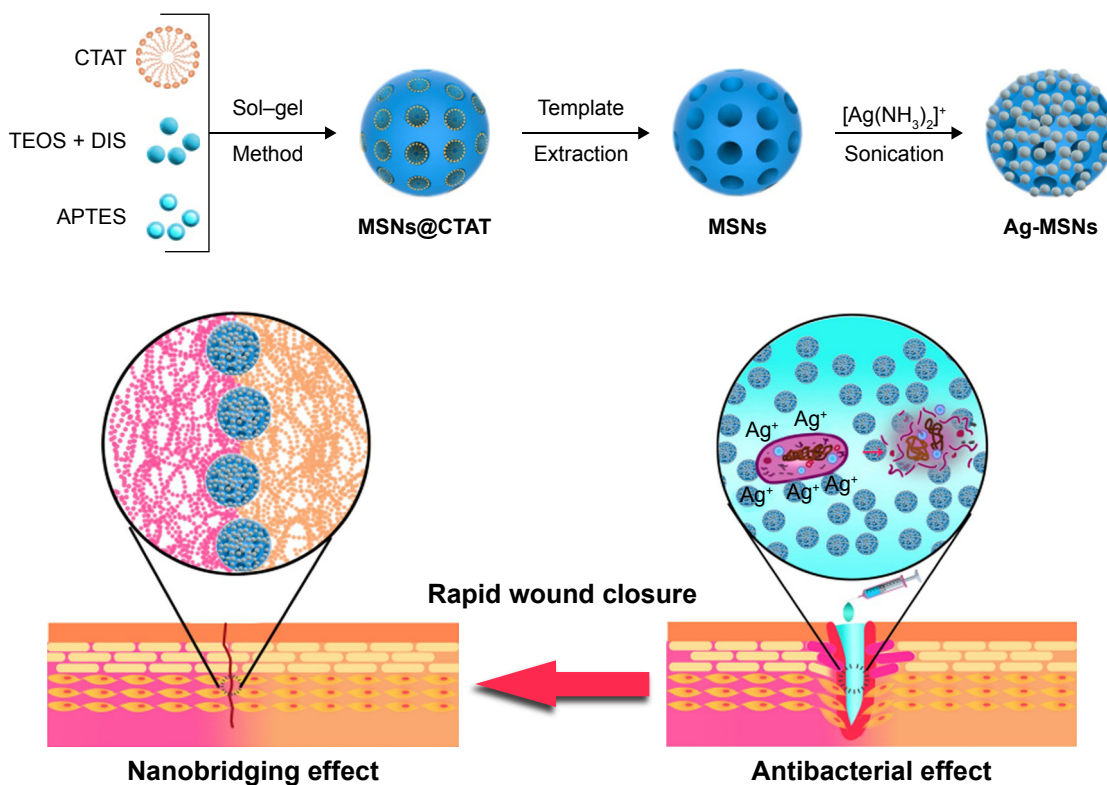
Results: Ag-MSNs exhibited not only strong adhesive properties but also excellent antibacterial activities than that of MSNs. Importantly, this antibacterial nano-adhesive achieved rapid and efficient closure and healing of wounds in comparison to sutures or MSNs in a mouse skin wound model. Furthermore, Ag-MSNs with fast degradable behavior caused little cellular toxicity and even less systemic toxicity during wound healing.

Conclusion: Our findings suggest that biodegradable Ag-MSNs can be employed as the next generation of nano-adhesives for rapid wound closure and aesthetic wound healing.

Keywords: nanosilver-decorated mesoporous silica nanoparticles, nano-adhesive, wound healing, antibacterial, biodegradable

Introduction

Wound closure and reconnection of injured tissues after surgery or trauma remains a challenge due to the complexity of healing.¹⁻³ Although various tissue adhesives designed to facilitate wound healing are gaining growing popularity in diverse clinical applications, they present significant inherent limitations such as rejection, infections, toxicity and/or excessive swelling.^{4,5} Furthermore, some of these adhesives are difficult to conform to deep, narrow wounds or wounds of irregular shapes.^{6,7} Consequently, it is highly desired to explore ideal tissue adhesives which employ biocompatible materials for adequate and rapid adhesion, accelerated wound closure and protection against infections. In addition to improving the mechanical properties and adhesive strength by the synthetic polymers,⁸⁻¹¹ inorganic nanoparticles (NPs) themselves are known as tissue adhesives owing to the so-called “nanobridging effect” between numerous protein chains



Scheme 1 Schematic representation of synthetic diagram for Ag-MSNs and their nanobridging and antibacterial effect for rapid wound closure.

Abbreviations: Ag-MSNs, nanosilver-decorated mesoporous silica nanoparticles; APTES, 3-aminopropyltriethoxysilane; CTAT, etyltrimethylammonium tosylate; DIS, bis(3-triethoxysilyl propyl)disulfide; TEOS, tetraethyl orthosilicate.

in the wound.^{12–18} It has been recently reported that several inorganic NPs including silica NPs, magnetic NPs and metal NPs exhibit strong adhesive properties in the wound closure of animal models.^{13–18} This novel strategy is advantageous in terms of cost, efficiency and convenience for clinical translation when compared with traditional polymer-based tissue adhesion methods.¹² However, a few studies have reported the antibacterial effects of these inorganic tissue adhesives.¹⁷ Hence, multifunctional NPs that integrate nanobridge effects and antibacterial properties have been highlighted as a promising tissue adhesive for safe and efficient wound healing.

Among several inorganic nano-adhesives, mesoporous silica NPs (MSNs) have received considerable attention in biomedical applications due to their highly specific surface area, vast surface functionalization capabilities and excellent biocompatibility.^{19–25} On the other hand, silver NPs (Ag NPs) are considered to be an efficient and broad-spectrum antibacterial tissue additive.^{26–30} However, low dispersity and slow silver ion release of Ag NPs limit their practical applications.^{29,30} To surmount these obstacles, Ag NPs can be easily embedded within MSNs or decorated on MSNs to form Ag-containing MSNs which can protect the Ag NPs from aggregation and release Ag ions in a controlled manner.^{27,31–33} Moreover, direct incorporation of a disulfide bond into the

framework of MSNs could facilitate their clinical translation as compared to traditional MSNs because of the fast and controllable biodegradation behavior.^{34,35} With these findings in mind, we hypothesized that disulfide bond-bridged Ag-MSNs may be employed as an effective and safe tissue adhesive with antibacterial and degradable properties for wound closure and healing, which has never been reported yet.

In the present study, we report on the facile synthesis of Ag-MSNs by controlled reduction of ultra-small nanosilvers onto both the surface and the large pore of biodegradable MSNs. We endeavor to examine the tissue adhesive property, antibacterial effect, biodegradability and biocompatibility of Ag-MSNs, as well as the subsequent treatment effects of Ag-MSNs in a rat wound closure model (Scheme 1). Given the combination of MSN-based tissue adhesive properties and decorated Ag NPs-induced bacterial killing and prevention, the antibacterial tissue adhesive Ag-MSNs might become the next generation of multifunctional tissue nano-adhesives for fast, safe and efficient wound healing.

Materials and methods

Materials

MTT, DMEM and FBS were obtained from Thermo Fisher Scientific (Waltham, MA, USA). Luria–Bertani (LB) broth

was purchased from Thermo Fisher Scientific. Gelatin, tetraethyl orthosilicate (98%), hexadecyltrimethylammonium bromide, 3-aminopropyltriethoxysilane and triethanolamine were purchased from Sigma-Aldrich Co. (St Louis, MO, USA). Bis(3-triethoxysilyl propyl)disulfide was purchased from Capatue Chemical Co., Ltd (Nanjing, China). Silver nitrate (AgNO_3 , 99.5%), dimethyl sulfoxide, *N,N*-dimethylformamide, hydrochloric acid (HCl, 37%) and ammonium hydroxide (NH_4OH , 28%) were purchased from Beijing Chemical Reagent Co. (Beijing, China).

Synthesis of MSNs and Ag-MSNs

The amino-modified MSNs of a small size were prepared via a modified one-pot method.³³ In a typical sol-gel reaction, 1.0 g of hexadecyltrimethylammonium bromide was dissolved in 100 mL of triethanolamine solution (0.5% w/w) and stirred at 80°C for 1 hour. Then, a mixture of 0.6 g of tetraethyl orthosilicate, 0.8 g of bis(3-triethoxysilyl propyl) disulfide and 0.1 g of 3-aminopropyltriethoxysilane was quickly added into the above solution and stirred vigorously for another 4 hours at the same temperature. The product was collected and washed with ethanol three times for surfactant removal. The as-prepared MSNs- NH_2 were dissolved in 95 mL of ethanol and HCl (37%, 5 mL) and stirred at 80°C for 12 hours. The final products were thoroughly washed with ethanol and deionized water three times.

Ag NPs-decorated MSNs were prepared according to our previously reported ultrasonication-assisted method.^{23,33} In brief, 100 mg of MSNs- NH_2 was dissolved in 45 mL of deionized water under ultrasonic treatment for 1 hour. Then, the silver ammonia complex cation $[\text{Ag}(\text{NH}_3)_2]^+$ was prepared by the mixture of 4.5 mL of 5% AgNO_3 solution and 0.5 mL of NH_4OH , and the silver ammonia complex cation mixture was added into the above solution. The mixture was reacted in the dark for 30 minutes under ultrasonication. The Ag-MSNs were collected and washed with deionized water three times.

To obtain negatively charged MSNs and Ag-MSNs, 100 mg of MSNs- NH_2 or Ag-MSNs was dispersed into 500 mL of *N,N*-dimethylformamide solution containing 2 wt% succinic anhydride and 1 mL of dimethyl sulfoxide. Then, the mixture was stirred at room temperature overnight. After that, the carboxylate-functionalized NPs were collected and washed with deionized water three times.

Characterization

Transmission electron microscopy (TEM) images were captured through a JEM-2100F transmission electron microscope (JEOL, Tokyo, Japan). Energy-dispersive X-ray spectroscopy (EDX) was also performed using a JEM-2100F

EDX instrument. X-ray powder diffraction investigation was carried out on a Rigaku X-ray diffractometer using Cu $K\alpha$ radiation. The Barrette-Emmett-Teller (BET) method was utilized to calculate the BET surface areas, total pore volume and Barre-Joyner-Halenda (BJH) pore diameter through Micromeritics ASAP2010 surface area analyzer. The size distribution and zeta potential were measured by Zetasizer (Nano ZS; Malvern Instruments, Malvern, UK).

Adhesion strength test

The gelatin hydrogel was selected as a traditional model to test the adhesion to biological tissue.¹⁷ The hydrogel was prepared by dissolving gelatin into deionized water at a concentration of 23% (wt%) and spread on a glass plate at 4°C overnight. The gelatin films were cut into several pieces with the size of 30×5×3 mm³ before use. Two films were attached with an overlap length of 10 mm and pressed for 30 seconds after the addition of 10 μL of nano-adhesive solution (20% w/w) containing the obtained MSNs or Ag-MSNs. Then, the tensile tests were performed on an Instron 5543 Tensile Meter (Instron Testing Systems, Norwood, MA, USA) with a load of 10 N and speed of 10 mm/min. At least six samples were examined for each group and the failure forces were calculated. Fresh cow liver was chosen as the tissue model for adhesion test. After cutting into two slices with desirable dimension of 30×10×3 mm³, their surfaces were dried using tissue paper. Then, a small drop of 10 μL of nano-adhesive solution (20% w/w) was added onto the liver surface and pressed for 30 seconds before testing.

Antibacterial assay

Standard strains of *Staphylococcus aureus* and *Escherichia coli* were obtained from the archival collection of Jilin University and cultivated at 37°C in LB medium. Gram-positive bacteria *S. aureus* and Gram-negative bacteria *E. coli* were diluted with LB medium for further experiments. To measure the dose-dependent antibacterial kinetics, Ag-MSNs of different concentrations (50, 25, 12.5, 6.25, 3.125 and 0 $\mu\text{g}/\text{mL}$) were separately added into tubes containing 5 mL of bacterial cultures and shaken at 200 rpm. At different time intervals (0, 1, 2, 3, 4, 5, 6, 9, 12, 18 and 24 hours), 100 μL of medium was collected to detect the OD value at 600 nm. The minimum inhibitory concentration (MIC) was obtained from the antibacterial kinetics.

Cytotoxicity assessment

Human skin keratinocytes (HaCaT) and mouse embryonic fibroblasts (NIH-3T3) were purchased from ATCC. Cells were cultured and maintained in DMEM media supplemented with

10% FBS at 37°C in an atmosphere containing 5% CO₂ and 100% relative humidity. For the in vitro cytotoxicity assay, cells in a logarithmic growth phase were seeded on a 96-well plate at a density of 5,000 cells per well. The cells were treated with different concentrations (100, 50, 25, 12.5, 6.25, 3.125 and 1.5625 µg/mL) of Ag-MSNs. After 24 hours of incubation, 20 µL of MTT solution were added to each well and the cells were incubated for another 2 hours at 37°C. The OD₄₉₀ was measured, and the cell viability ratio was calculated.

Degradation study

To mimic the physiological conditions in the body, degradation of MSNs or Ag-MSNs (100 µg/mL) was evaluated in simulated body fluid (SBF) containing 10 mM glutathione (GSH) at 37°C in a constant temperature shaker bath. At predetermined times points (0, 6, 12, 24, 48, 72 and 96 hours), samples were collected and centrifuged at 10,000 rpm for 10 minutes. The supernatant was collected and the content of Si was analyzed via inductively coupled plasma optical emission spectrometry (ICP-OES); the degradation rate was then calculated. In addition, TEM images were taken at 48 hours of incubation.

In vivo wound healing and safety evaluation

Male Wistar rats (210–230 g) were purchased from the Experimental Animal Center of Jilin University and were maintained in a conventional animal housing facility throughout the experiment. All animal experimental protocols were approved by the Ethics Committee for the Use of Experimental Animals of Jilin University. The experimental manipulation of mice was conducted in accordance with the National Institute of Health Guide for the Care and Use of Laboratory Animals and the approval of the Scientific Investigation Board of Science and Technology of Jilin Province (Changchun, China). Two parallel cutaneous incisions 1 cm in length were made on the abdomen of the rat under anesthesia. For the left wounds, closure sutures were made according to the clinical gold standard. For the right wounds, 10 µL of MSN or Ag-MSN solution (20% w/w) was added to the wound by a pipette. The wounds were pressed at the edges from both sides by fingers for 30 seconds and the excessive nano-adhesive was removed. The rats were divided to three groups (n=6) including control, MSNs and Ag-MSNs (right wound), and every rat in each group had a sutured positive control wound (left wound). Macroscopic images of the wound site of each rat were taken at 1, 3 and 5 days, and the wound widths were measured.

After 5 days of treatment, all the rats were sacrificed after their blood samples were collected by heart puncture. The hematological parameters were examined with

a hemocytometer (Coulter STKS; Coulter Corp., Hialeah, FL, USA). Serum samples were separated after overnight coagulation of the blood, and the biochemical parameters were analyzed automatically with the Coulter LX2D (Beckman, Brea, CA, USA). The main organs (heart, liver, spleen, lungs and kidneys) and explanted tissues surrounding the skin wound were collected, washed and fixed. The paraffin sections were stained with H&E or Masson's trichrome. All images were examined under a digital microscope. Pathological analyses were conducted on these organs by two independent investigators blinded to the group assignment. The inflammation levels were scored referring 0 to no inflammatory cells, 1 to scattered inflammatory cell infiltrate within the stroma without lymphoid nodules, 2 to nonconfluent lymphoid nodules and 3 to large inflammatory areas with confluence of infiltrate. The amounts of collagen were scored as referring 0 to no collagen, 1 to minor collagen level, 2 to moderate collagen level and 3 to large amount of collagen.

Statistical analysis

The experimental results were analyzed with SPSS19.0 statistical software. Data are presented as the mean±SD. Statistical significance ($P<0.05$) was evaluated using Student's *t*-test when only two groups were compared. If more than two groups were compared, evaluation of significance was performed using one-way ANOVA, followed by Bonferroni's post hoc test.

Ethics statement

All animals received care in compliance with the guidelines outlined in the Guide for the Care and Use of Laboratory Animals and the procedures were approved by the Jilin University of China Animal Care and Use Committee.

Results and discussion

The amino-functionalized, disulfide bond-bridged MSNs with a smaller size of 52.3±5.2 nm were synthesized through a modified sol-gel reaction (Figure 1A and Figure S1). After MSNs-NH₂ were generated, small Ag NPs were grown on the silica surface through a facile ultrasonication-assisted method.^{33,36} TEM images show Ag-MSNs with an overall size of 61.8±7.3 nm decorated with Ag NPs of 3.3±0.8 nm (Figure 1B and Figure S1). Ag-MSNs are stable in water and show a lower polydispersity index (0.196), with a negative surface charge (−28.5±3.4 mV) due to their carboxyl group (Table S1). These findings indicate that the well-synthesized Ag-MSNs protect against the aggregation of Ag NPs and may inhibit bacterial growth due to the release of silver ions. MSNs exhibited similar physicochemical properties to

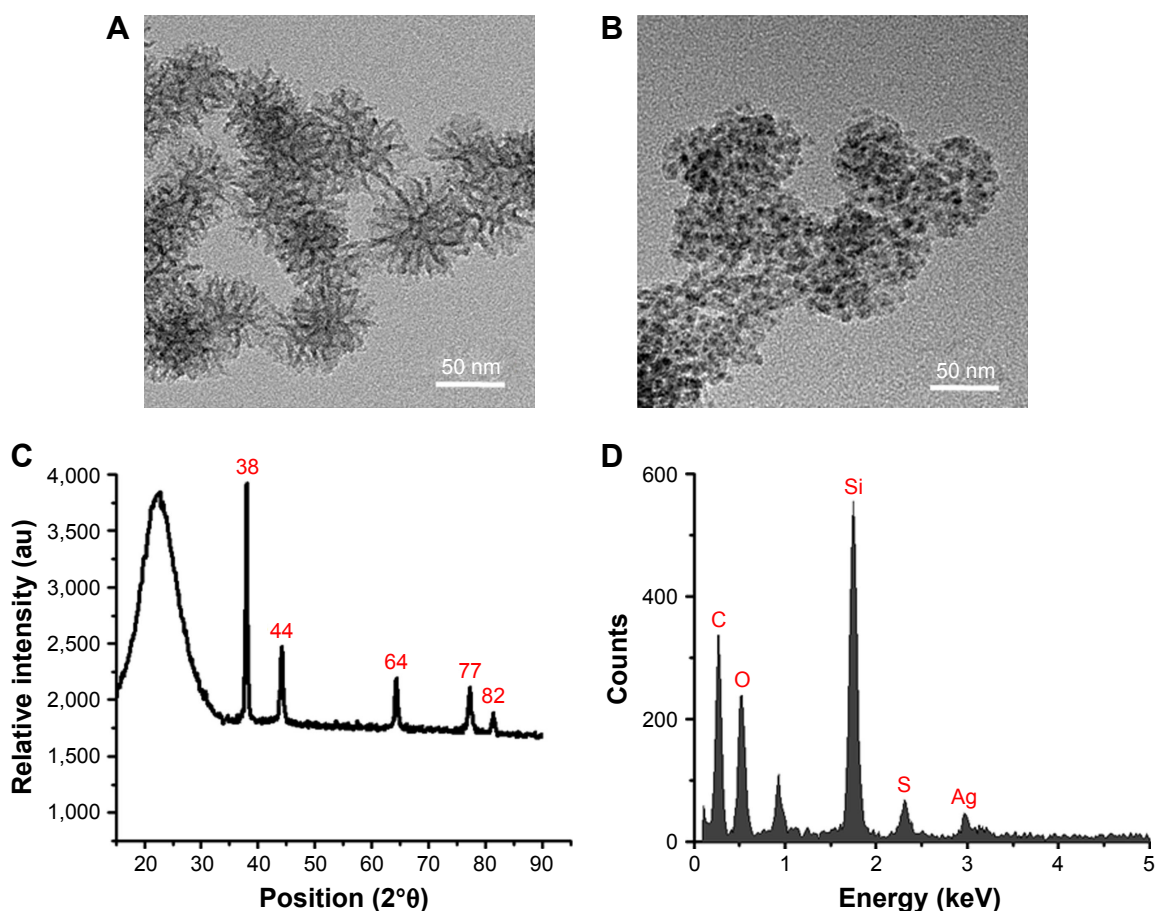


Figure 1 Characterization of nano-adhesives.

Notes: TEM images of (A) MSNs and (B) Ag-MSNs. (C) XRD patterns and (D) EDS spectra of Ag-MSNs.

Abbreviations: Ag-MSNs, nanosilver-decorated mesoporous silica nanoparticles; EDS, energy-dispersive X-ray spectrometer; MSNs, mesoporous silica nanoparticles; TEM, transmission electron microscope; XRD, X-ray powder diffraction.

those of the Ag-MSNs, which allows the comparison of the biological properties of the two nano-adhesives. As shown in Figure 1C, the five classic diffraction peaks at the 2θ values of 38° , 44° , 64° , 77° and 82° correspond to the (111, 200, 220, 311) and (222) crystallographic planes of silver, while a broad peak in the range from 15° to 30° might be attributed to the amorphous silica. EDX spectroscopy analysis further demonstrated the presence of silver, as well as the coexistence of silicon, oxygen and carbon (Figure 1D). In addition, both the MSNs and Ag-MSNs exhibited a type IV isotherm (Figure S2). The BET surface area, total pore volume and BJH pore size of the Ag-MSNs were determined to be $506.8 \text{ m}^2/\text{g}$, $0.87 \text{ cm}^3/\text{g}$ and 4.1 nm , respectively (Table S1). As expected, the mesoporous parameters of Ag-MSNs were lower than those of MSNs ($623.2 \text{ m}^2/\text{g}$, $1.35 \text{ cm}^3/\text{g}$ and 6.6 nm), which suggests the presence of Ag NPs in the interior and surface of the MSNs.

As a denatured form of collagen, gelatin is a natural component in human skin, which has been widely used in tissue engineering.³⁷ Hence, gelatin hydrogels were selected as a

model material to test the adhesive properties of the MSNs and Ag-MSNs. In the adhesion strength test, two gelatin ribbons ($30 \times 5 \times 3 \text{ mm}^3$, length \times width \times thickness) were adhered together by gently pressing for 30 seconds after spreading $15 \mu\text{L}$ of the MSN or Ag-MSN solution (20% w/w). As shown in Figure 2A, their shape indicates a rupture event at the peak of each curve, where the failure forces built up until the gelatin ribbons ripped at the glued site. To further account for the large deviation of failure forces, six samples were measured for each type of nano-adhesives. As shown in Figure 2B, the joint of the gelatin–gelatin film yields a failure force of 20 mN without the addition of an NP solution. The failure force with the application of MSNs and Ag-MSNs was significantly increased by 6- to 8-fold and was 120 mN and 160 mN, respectively. It is worth noting that silver NPs decoration could significantly increase the adhesion strength of the MSNs, which might be attributed to specific interactions such as hydrogen bonding from the rough surface that strengthen the adsorption of NPs to the gel surface.¹³ The adhesive function of nano-adhesives was

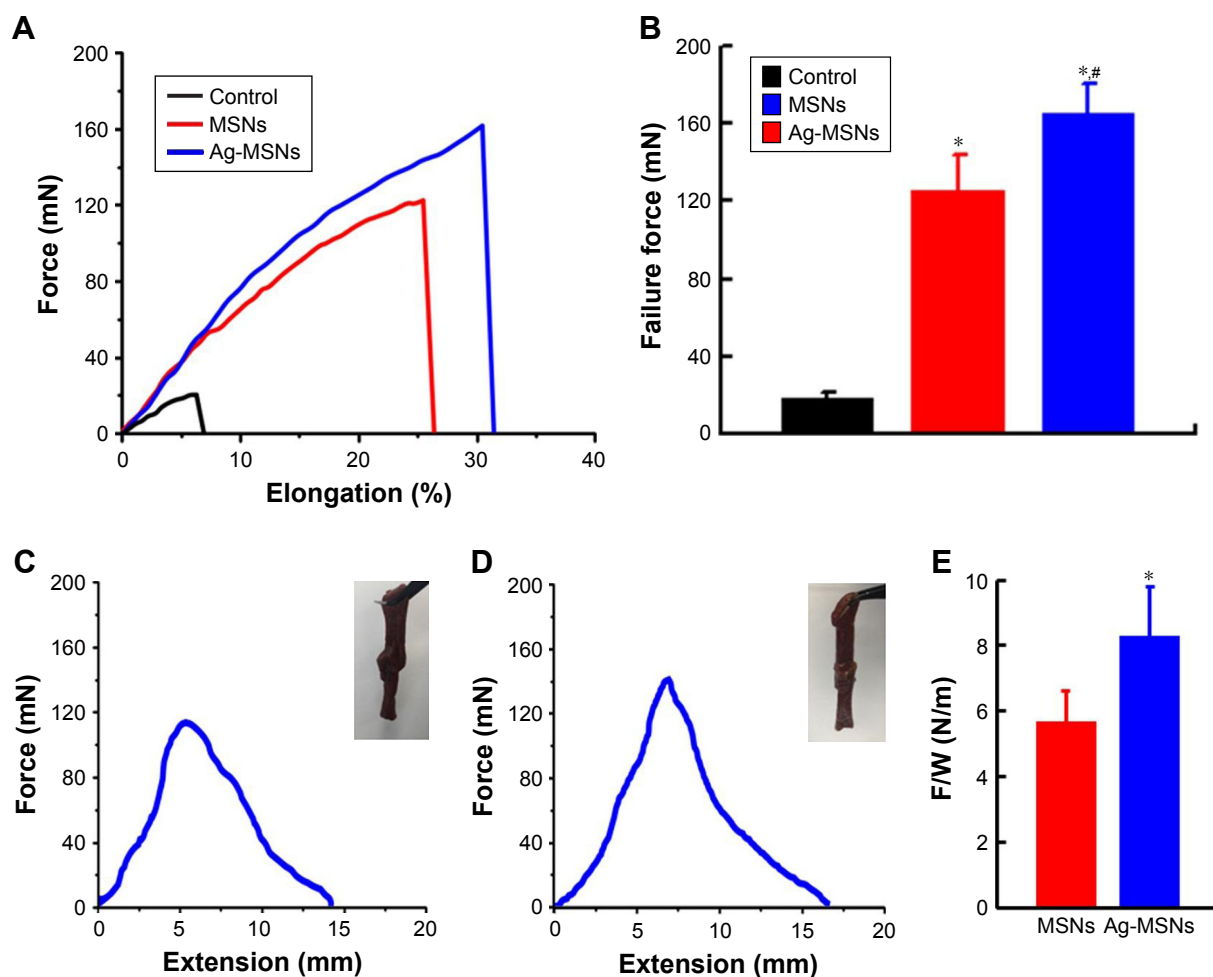


Figure 2 Tissue adhesive properties of nano-adhesives.

Notes: (A) Normalized force–distance curves for the lap joints glued with gelatin films. (B) Failure forces of gelatin–gelatin film glued by MSNs or Ag-MSNs. These data represent six separate experiments and are presented as the mean values \pm SD, * P <0.05 vs control group, # P <0.05 vs MSNs group. Representative force–distance curves of liver tissues glued by (C) MSNs and (D) Ag-MSNs. Insets indicate nano-adhesive holds the two liver slices together. (E) Failure force, F , normalized by the width of the joint, W , for lap joints glued using solutions of MSNs or Ag-MSNs. These data represent six separate experiments and are presented as the mean values \pm SD, * P <0.05 vs MSNs group.

Abbreviations: Ag-MSNs, nanosilver-decorated mesoporous silica nanoparticles; MSNs, mesoporous silica nanoparticles.

further confirmed by testing the attachment of two cow liver slices. As shown in Figure 2C–E, Ag-MSNs exhibited higher maximum adhesive force than MSNs, indicating that nanosilver decoration has a positive influence on tissue adhesive function. It is worth to note that the adhesion force of both MSNs and Ag-MSNs was concentration dependent, which increased with the increase of nano-adhesive concentration (Figure S3). We speculated that the enriched carboxyl groups on the nano-adhesive's surface might play a crucial role in facilitating the nanobridging effect.¹³ Future studies are needed to elucidate the mechanism of the effect of surface modification on adhesion. Collectively, these in vitro adhesion findings indicate that both MSNs and Ag-MSNs might be suitable nano-adhesives for wound closure.

Gram-positive bacteria *S. aureus* and Gram-negative bacteria *E. coli* were employed to investigate the antibacterial

activity of the nano-adhesives because they are well-known candidates involved in wound infections.³⁸ We first evaluated the bacterial growth kinetics of *S. aureus* and *E. coli* in liquid LB media with Ag-MSNs by measuring the OD₆₀₀ after culture from 1 to 24 hours. As shown in Figure 3, initial growth of both *S. aureus* and *E. coli* was time-dependently delayed and dose-dependably reduced with increasing concentrations of Ag-MSNs. Importantly, the corresponding MIC of Ag-MSNs for *E. coli* was 12.5 μ g/mL, which was lower than that for *S. aureus* (25 μ g/mL). These findings are mainly because Gram-positive bacteria with thicker and more compact walls are more stable than Gram-negative bacteria.³⁹ It was reasonable to reveal that *E. coli* was more sensitive to Ag-MSNs than *S. aureus*, which also aligned with our previous work.³³ The excellent antibacterial activity of Ag-MSNs against both Gram-negative bacteria *E. coli* and

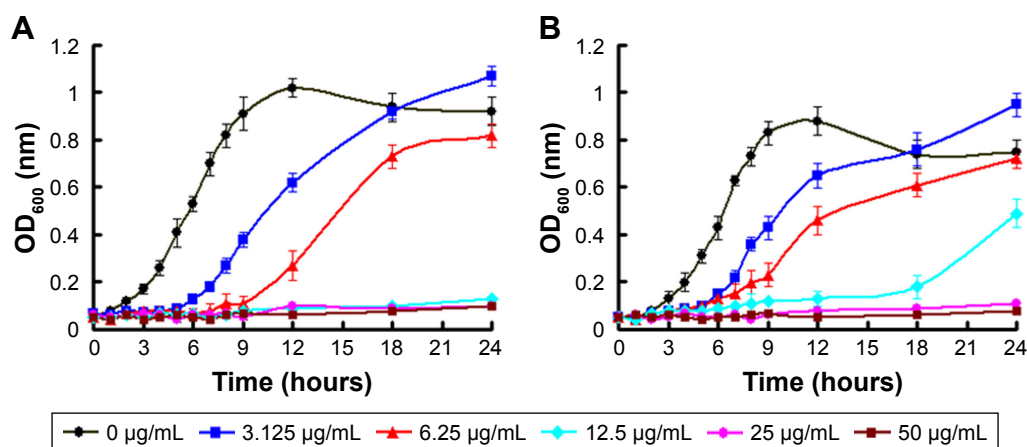


Figure 3 Bacterial growth curve of (A) *Escherichia coli* and (B) *Staphylococcus aureus* in LB liquid medium in the presence of Ag-MSNs with different concentrations. These data represent three separate experiments and are presented as mean values \pm SD.

Abbreviations: Ag-MSNs, nanosilver-decorated mesoporous silica nanoparticles; LB, Luria-Bertani.

Gram-positive bacteria *S. aureus* might benefit from the protection of Ag NPs aggregation, as well as the fast release of bactericidal silver ions.⁴⁰

Since silica NPs are highly biocompatible and approved by the US Food and Drug Administration, one of the major hurdles for intracorporeal use of Ag-MSNs is its chronic toxicity and the inflammatory effects induced by the released silver ions.^{41,42} However, silver-containing wound dressings are frequently used as effective and safe agents for treating wounds that are clinically infected or at risk of infection.⁴³ Our previous reports have further shown that Ag-MSNs are capable of reducing the release of silver ions, resulting in lower toxicity.^{23,33} To ensure the biocompatibility of nano-adhesives, their cytotoxicity was determined on human skin keratinocytes (HaCaT) and mouse embryonic fibroblasts (NIH-3T3) via the MTT assay. As shown in Figure 4A and B, the viability of both HaCaT and NIH-3T3 cells incubated with Ag-MSNs decreased in a dose-dependent manner, while those cells incubated with MSNs exhibited no cytotoxicity even when exposed to concentrations up to 100 μ g/mL. It is worth noting that Ag-MSNs at 12.5 μ g/mL do not affect cell viability, indicating their good biocompatibility at their MIC. We attributed this phenomenon to the slow-release behavior Ag-MSNs in the neutral microenvironment of normal cells, according to our previously reported data.³³

Since the clinical application of traditional MSNs was restricted by their lower and uncontrolled degradation rate, the design of MSNs with biodegradable behavior was highly desired.^{44,45} It is well known that disulfide bond can be specifically sensitive to the reducing microenvironment intracellularly, which endows fast degradability of

disulfide-bridged MSNs.^{34,35} The degradation profile of two nano-adhesives was studied in SBF containing 10 mM GSH to mimic intracellular and extracellular microenvironment. As shown in Figure 4C, both MSNs and Ag-MSNs showed overall faster and time-dependent degradation; they began to degrade into fragments in 48 hours (Figure 4D and E). In contrast, nano-adhesives exhibited slower degradation rate in pure SBF, further identifying their GSH-accelerating degradation behavior *ex vitro* and *in vitro*.³⁵ Moreover, Ag-MSNs showed similar manner of degradation as MSNs, indicating that nanosilver decoration has negligible influence on its degradability. It should be mentioned that this degradation test was done under static conditions, while *in vivo* settings were dynamic under the balance between oxidized (GSSG) and reduced GSH.⁴⁶ Therefore, we indicate that the degradation of nano-adhesives *in vivo* might be higher than that *in vitro* due to the constant concentration of GSH.

Aside from the *in vitro* adhesion, antibacterial, toxicity and degradation tests, an *in vivo* experiment is indispensable for evaluating the real wound healing effect of potential nano-adhesives. Two parallel full-thickness cutaneous incisions 1 cm in length were made on the abdominal skin of the rat. For the left wounds, closure sutures were made to mimic the clinical gold standard. In comparison, 10 μ L of MSN or Ag-MSN solution (20% w/w) was applied to the right wound using pipettes (Figure S4). We pressed both sides of the wound for 30 seconds, and the excess solution was removed with a compress. As shown in Figure 5A, the wound areas reduced progressively, and less wound leakages or infections were observed after bridging with the two nano-adhesives. At the end of the treatment, the wounds were esthetically healed in both the MSN and Ag-MSN solution-treated groups,

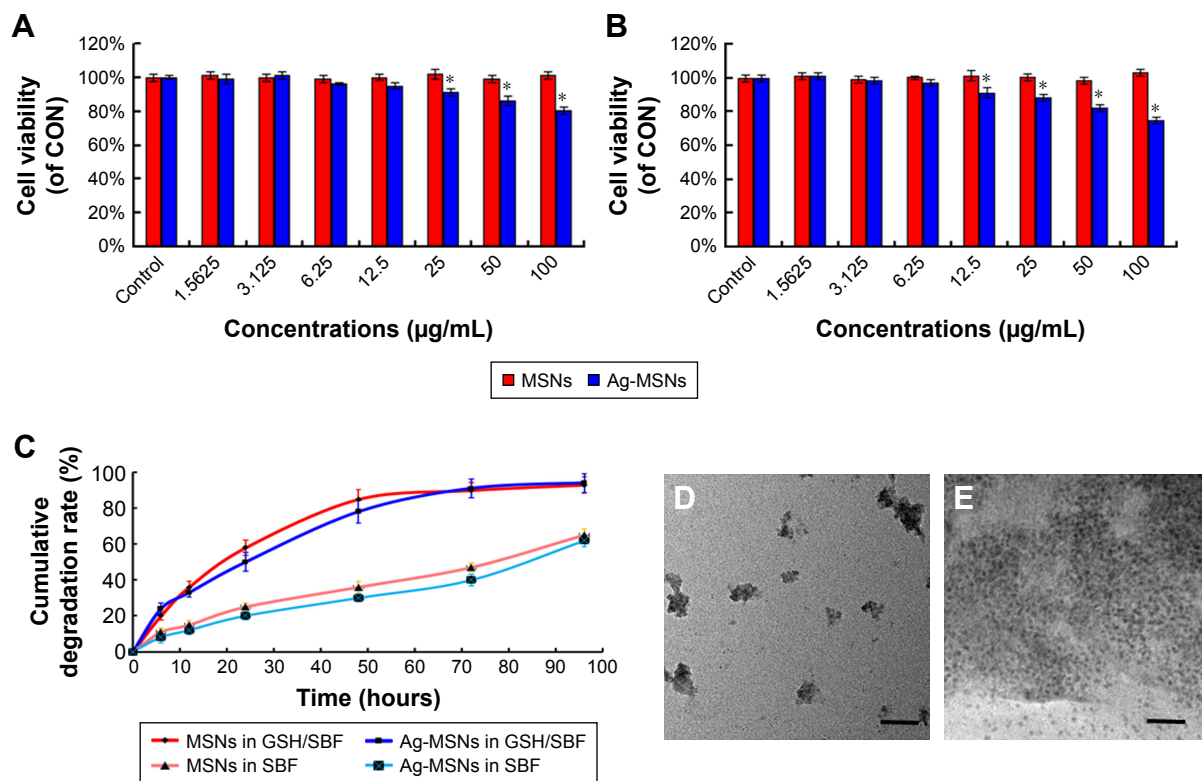


Figure 4 Biocompatibility and biodegradability of nano-adhesives.

Notes: The cytotoxicity of MSNs and Ag-MSNs against (A) HaCaT cells and (B) NIH-3T3 cells at different levels of concentration after 24 hours. (C) Cumulative degradation profile of MSNs and Ag-MSNs under 10 mM GSH-containing SBF for 96 hours. These data represent three separate experiments and are presented as mean values±SD. *P<0.05 vs control group. TEM images of (D) MSNs and (E) Ag-MSNs after 48 hours of incubation in SBF containing 10 mM GSH; the scale bars represent 50 nm.

Abbreviations: Ag-MSNs, nanosilver-decorated mesoporous silica nanoparticles; GSH, glutathione; MSNs, mesoporous silica nanoparticles; SBF, simulated body fluid; TEM, transmission electron microscope.

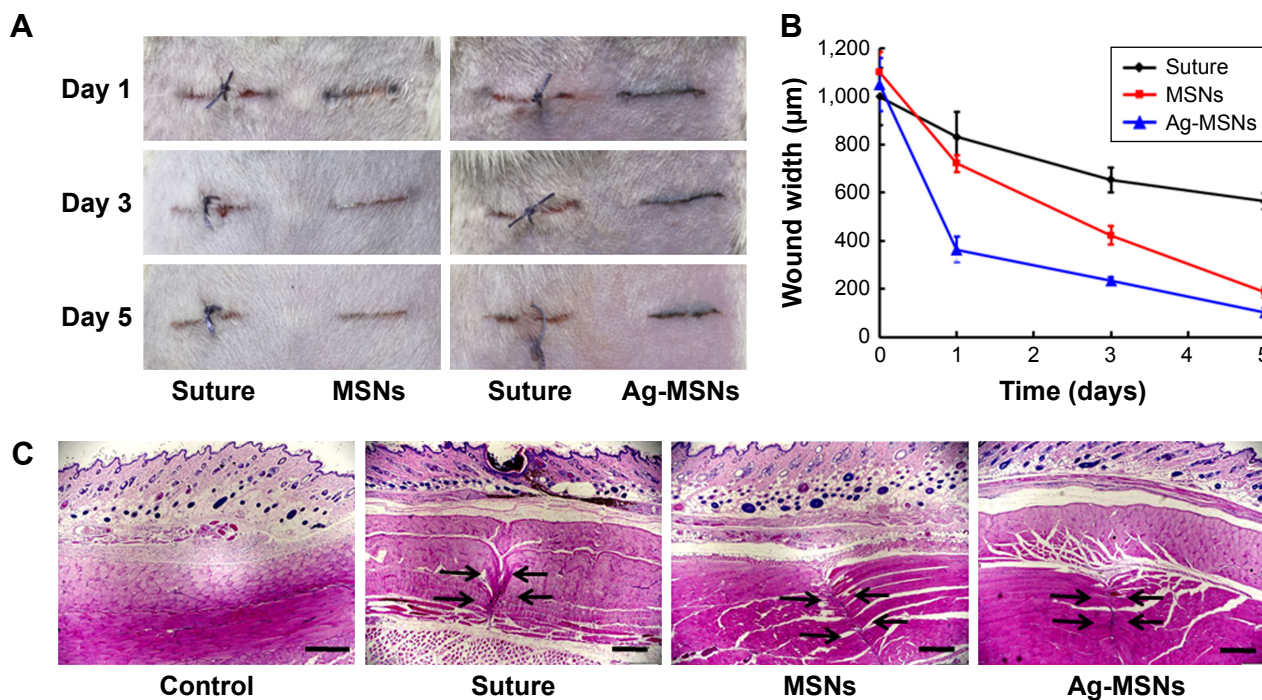


Figure 5 In vivo wound healing performance of nano-adhesives.

Notes: (A) Representative macroscopic images of the wound healing treated by ethicon suture or nano-adhesives (MSNs and Ag-MSNs) in a Wistar rat model for 5 days. (B) Measurement of the width between the borders of the wound area after 5 days. The values represent the mean values±SD, n=6. (C) H&E staining images of normal skin treated with ethicon suture, MSNs and Ag-MSNs at day 5 post-wounding. The scale bars represent 500 µm. The arrows indicate the wound edges.

Abbreviations: Ag-MSNs, nanosilver-decorated mesoporous silica nanoparticles; MSNs, mesoporous silica nanoparticles.

whereas this did not occur for the groups treated with water and closure sutures. Importantly, faster reduction in wound width was observed in Ag-MSN group rather than the MSN group, indicating its better performance of wound healing (Figure 5B). Skin tissues possess similar properties to hydrogels, such as flexibility, an interconnected porous structure and abundant water content.⁴⁷ Our nano-adhesive could absorb numerous protein chains in the extracellular matrix of the skin tissue through hydrogen bonding, which acted as nanobridges between the network structures.¹³ Furthermore, the nano-adhesive is easier and more effective than suturing, because the removal of sutures requires trained personnel and operation time and adds to local trauma that delays wound healing.⁴⁸ The histopathologic changes on day 5 are shown in Figure 5C. As expected, most of the wound edges were bonded correctly in the nanobridging groups, but not in the untreated group, while new connective matrix formed by granulation tissue was observed in the suturing group. It is worth noting that Ag-MSNs exhibited better performance in esthetic wound healing than MSNs. Substantial migration of inflammatory cells was observed in the suture group,

while less inflammatory cell infiltration was observed in the nano-adhesive group (Figure 6A and C). It is worth noting that wound closure treated with Ag-MSNs revealed less pathologic inflammation than that treated with the MSNs, which might be attributed to the above-demonstrated antibacterial activity. Furthermore, Masson's trichrome staining suggested decreased collagen distribution with either MSN or Ag-MSN treatment compared to suturing at day 5 (Figure 6B and D), indicating a faster wound healing process mediated through nano-adhesives. Taken together, Ag-MSNs achieved easier and esthetic wound closure *in vivo* with less inflammation.

In addition to the favorable biodegradation behavior of nano-adhesives, the *in vivo* biocompatibility was evaluated comprehensively through body weight, hematological and biochemical examinations, as well as organ histopathology analyzed after application of MSNs or Ag-MSNs for 5 days in the above rat model. As shown in Figure S5, no remarkable changes were observed in the body weight of any of the groups. We selected red blood cells, white blood cells, platelet, lymphocyte, monocyte, mean corpuscular hemoglobin, mean corpuscular volume and hemoglobin as the

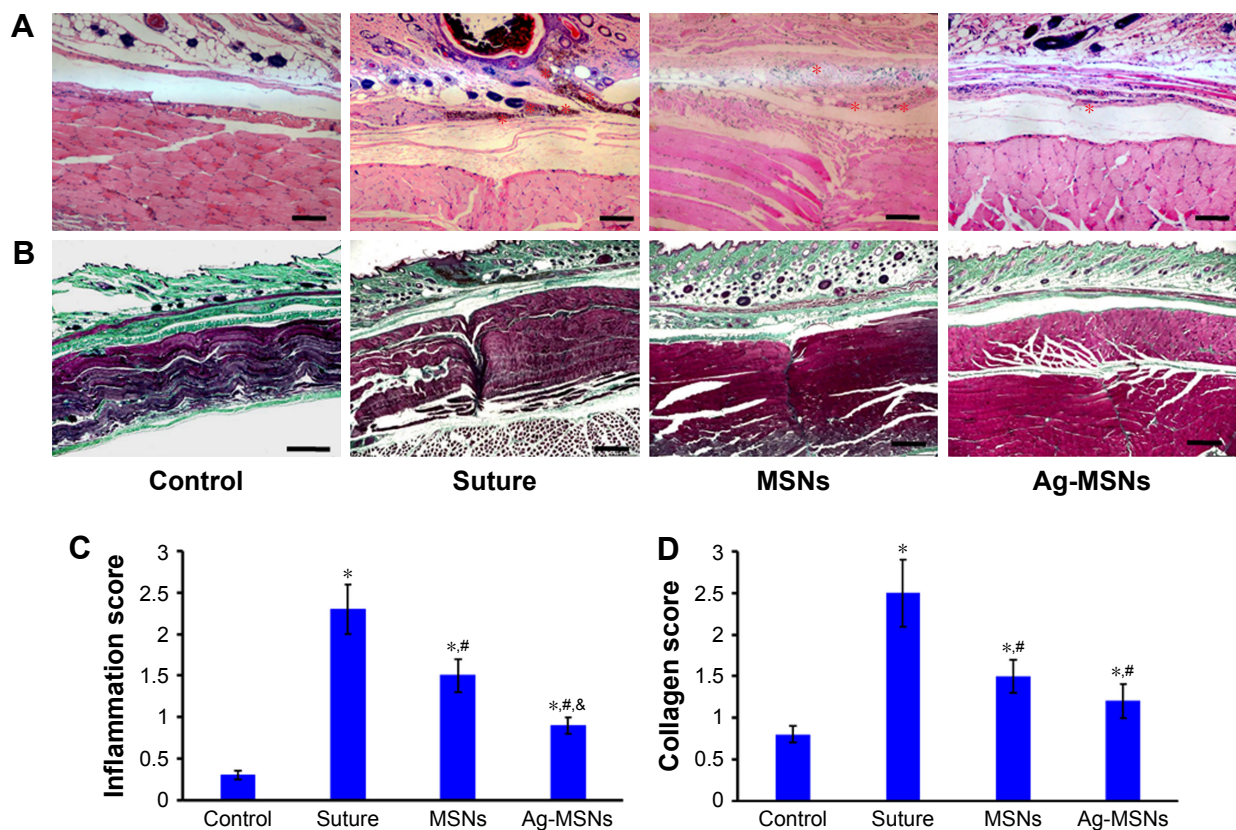


Figure 6 *In vivo* wound healing performance of nano-adhesives.

Notes: Representative (A) H&E staining and (B) Masson's trichrome staining images of normal skin treated with ethicon suture, MSNs and Ag-MSNs at day 5 post-wounding. The scale bars represent 200 and 500 μ m for (A and B), respectively. The stars indicate inflammatory cells. (C) Inflammatory responses of the wound area according to the pathology criteria (score 0–3). (D) Levels of collagen formed at the wound area were measured according to the pathology criteria (score 0–3). The values represent mean values \pm SD, n=6. * P <0.05 vs control group, # P <0.05 vs suture group, & P <0.05 vs MSNs group.

Abbreviations: Ag-MSNs, nanosilver-decorated mesoporous silica nanoparticles; MSNs, mesoporous silica nanoparticles.

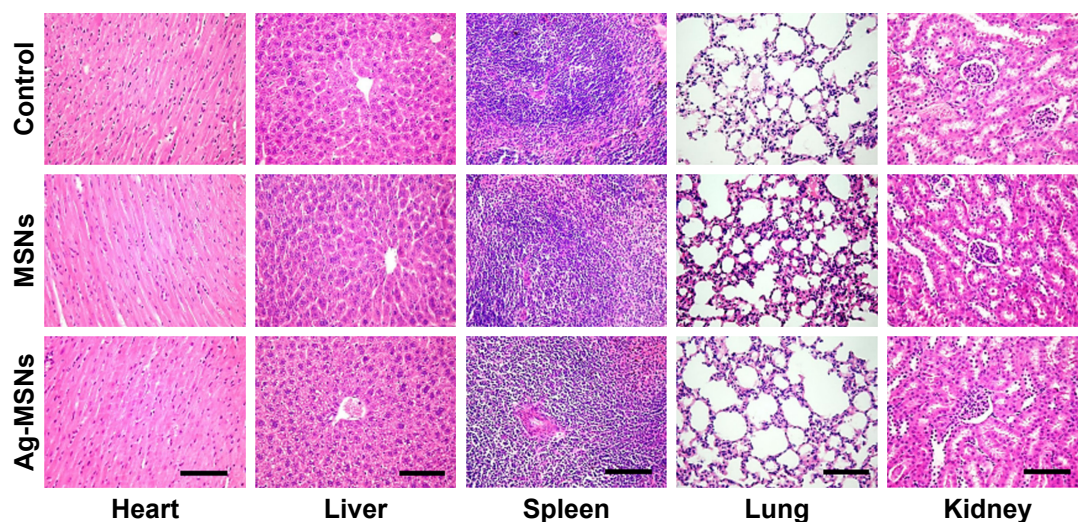


Figure 7 H&E staining images of the heart, liver, spleen, lung and kidney of rats from each group.

Note: The scale bars represent 100 μm .

Abbreviations: Ag-MSNs, nanosilver-decorated mesoporous silica nanoparticles; MSNs, mesoporous silica nanoparticles.

hematological parameters to study the hematological toxicity of nano-adhesives. There was no significant difference in the hematological parameters of the MSN- or Ag-MSN-treated groups compared with the control group (Table S2). We further selected AST, ALT, alkaline phosphatase, albumin, blood urea nitrogen, creatinine, cholesterol and triglyceride as the biochemical parameters to monitor the functions of the vital organs after treatment with nano-adhesives. As expected, no obvious abnormalities were observed in the rats treated with MSNs or Ag-MSNs compared with the control groups (Table S3). In addition, histological examination of the heart, liver, spleen, lung and kidney of the rats was also conducted in this study. As shown in Figure 7, the microscopic examination of the all these tissues showed no remarkable differences between the treatment and control groups. Although all these findings implicated that both MSNs and Ag-MSNs did not exhibit any abnormal effects on all tested rats, a comprehensive study on the biodistribution and long-term toxicity of these nano-adhesives is still needed to fully understand their nano-bio interactions. Although ZnO NPs have been reported as antimicrobial tissue adhesive that exhibited successful wound closure and esthetic wound healing,¹⁷ the direct biocompatibility data of ZnO NP in vivo was not investigated. Compared to ZnO NPs, the Ag-MSNs in our study showed similar rapid wound closure and esthetic wound healing properties in vitro and in vivo. Importantly, we have systematically demonstrated that Ag-MSNs have good biocompatibility due to their biodegradable behavior. In addition, MSNs can be considered as a nanocarrier to load and controlled release drug to accelerate wound healing.

Conclusion

In summary, we designed and fabricated biodegradable and biocompatible nanosilver-decorated mesoporous silica NPs (Ag-MSNs) integrating tissue adhesive properties and antibacterial activity. As designed, the Ag-MSNs solution possessed a higher failure force between two gelatin films or liver slices than MSNs. Moreover, this nano-adhesive exhibited excellent antibacterial activity against both Gram-negative bacteria, *E. coli*, and Gram-positive bacteria, *S. aureus*. Importantly, Ag-MSNs achieved easy and esthetic wound closure in a rat model without inducing any infections or side effects. Given the needs of various tissue adhesives for clinical use, our results give additional insights into the biomedical applications of designed multifunctional inorganic NPs, which can be employed as nano-adhesives for efficient and safe wound closure and esthetic wound healing.

Acknowledgments

Mrs Qiuqing Wang is acknowledged for her help in preparing the paper. This work was supported by the National Natural Science Foundation of China (Grant No 81601609, 81771982, 61535010, 81371681, 81470778 and 8160071152), the Key Research Program of the Chinese Academy of Sciences (No KFZD-SW-210), the Natural Science Foundation of Jiangsu Province (No BE2015601) and the Science and Technology Commission Program of Nanjing (201605011).

Disclosure

The authors report no conflicts of interest in this work.

References

1. Armitage J, Lockwood S. Skin incisions and wound closure. *Surgery*. 2011;29(10):496–501.
2. Gause WC, Wynn TA, Allen JE. Type 2 immunity and wound healing: evolutionary refinement of adaptive immunity by helminths. *Nat Rev Immunol*. 2013;13(8):607–614.
3. Rowan MP, Cancio LC, Elster EA, et al. Burn wound healing and treatment: review and advancements. *Crit Care*. 2015;19(1):243.
4. Robson MC, Barbul A. Guidelines for the best care of chronic wounds. *Wound Repair Regen*. 2006;14(6):647–648.
5. Ghobril C, Grinstaff MW. The chemistry and engineering of polymeric hydrogel adhesives for wound closure: a tutorial. *Chem Soc Rev*. 2015;44(7):1820–1835.
6. Boateng J, Catanzano O. Advanced therapeutic dressings for effective wound healing – a review. *J Pharm Sci*. 2015;104(11):3653–3680.
7. Singer AJ, Clark RA. Cutaneous wound healing. *N Engl J Med*. 1999;341(10):738–746.
8. Azuma K, Nishihara M, Shimizu H, et al. Biological adhesive based on carboxymethyl chitin derivatives and chitin nanofibers. *Biomaterials*. 2015;42:20–29.
9. Peng B, Lai X, Chen L, et al. Scarless wound closure by a mussel-inspired poly(amidoamine) tissue adhesive with tunable degradability. *ACS Omega*. 2017;2(9):6053–6062.
10. Lee TT, Garcia JR, Paez JJ, et al. Light-triggered in vivo activation of adhesive peptides regulates cell adhesion, inflammation and vascularization of biomaterials. *Nat Mater*. 2015;14(3):352–360.
11. Brennan MJ, Kilbride BF, Wilker JJ, Liu JC. A bioinspired elastin-based protein for a cytocompatible underwater adhesive. *Biomaterials*. 2017;124:116–125.
12. Berthet M, Gauthier Y, Lacroix C, Verrier B, Monge C. Nanoparticle-based dressing: the future of wound treatment? *Trends Biotechnol*. 2017;35(8):770–784.
13. Rose S, PrevotEAU A, Elzière P, Hourdet D, Marcellan A, Leibler L. Nanoparticle solutions as adhesives for gels and biological tissues. *Nature*. 2014;505(7483):382–385.
14. Liu H, Peng Y, Yang C, Wang M. Silica nanoparticles as adhesives for biological tissues? Re-examining the effect of particles size, particle shape, and the unexpected role of base. *Part Part Syst Charact*. 2017;34(12):1700286.
15. Meddahi-Pellé A, Legrand A, Marcellan A, Louedec L, Letourneur D, Leibler L. Organ repair, hemostasis, and in vivo bonding of medical devices by aqueous solutions of nanoparticles. *Angew Chem Int Ed Engl*. 2014;53(25):6369–6373.
16. Shin K, Choi JW, Ko G, et al. Multifunctional nanoparticles as a tissue adhesive and an injectable marker for image-guided procedures. *Nat Commun*. 2017;8:15807.
17. Gao Y, Han Y, Cui M, Tey HL, Wang L, Xu C. ZnO nanoparticles as an antimicrobial tissue adhesive for skin wound closure. *J Mater Chem B*. 2017;5(23):4535–4541.
18. Matter MT, Starsich F, Galli M, et al. Developing a tissue glue by engineering the adhesive and hemostatic properties of metal oxide nanoparticles. *Nanoscale*. 2017;9(24):8418–8426.
19. Shao D, Li M, Wang Z, et al. Bioinspired diselenide-bridged mesoporous silica nanoparticles for dual-responsive protein delivery. *Adv Mater*. 2018;1801198.
20. Shao D, Li J, Zheng X, et al. Janus “nano-bullets” for magnetic targeting liver cancer chemotherapy. *Biomaterials*. 2016;100:118–133.
21. Shao D, Zhang X, Liu W, et al. Janus silver-mesoporous silica nano-carriers for SERS traceable and pH-sensitive drug delivery in cancer therapy. *ACS Appl Mater Interfaces*. 2016;8(7):4303–4308.
22. Shao D, Lu MM, Zhao YW, et al. The shape effect of magnetic mesoporous silica nanoparticles on endocytosis, biocompatibility and biodistribution. *Acta Biomater*. 2017;49:531–540.
23. Wang Z, Chang Z, Lu M, et al. Janus silver/silica nanoplateforms for light-activated liver cancer chemo/photothermal therapy. *ACS Appl Mater Interfaces*. 2017;9(36):30306–30317.
24. Liu G, Li Q, Ni W, et al. Cytotoxicity of various types of gold-mesoporous silica nanoparticles in human breast cancer cells. *Int J Nanomedicine*. 2015;10:6075–6087.
25. Wang Z, Shao D, Chang Z, et al. Janus gold nanoplateform for synergetic chemoradiotherapy and computed tomography imaging of hepatocellular carcinoma. *ACS Nano*. 2017;11(12):12732–12741.
26. Chernousova S, Epple M. Silver as antibacterial agent: ion, nanoparticle, and metal. *Angew Chem Int Ed Engl*. 2013;52(6):1636–1653.
27. Tian Y, Qi J, Zhang W, Cai Q, Jiang X, Facile JX. Facile, one-pot synthesis, and antibacterial activity of mesoporous silica nanoparticles decorated with well-dispersed silver nanoparticles. *ACS Appl Mater Interfaces*. 2014;6(15):12038–12045.
28. Chang ZM, Wang Z, Lu MM, et al. Janus silver mesoporous silica nanobullets with synergistic antibacterial functions. *Colloids Surf B Biointerfaces*. 2017;157:199–206.
29. Kvítek L, Panáček A, Soukupová J, et al. Effect of surfactants and polymers on stability and antibacterial activity of silver nanoparticles (NPs). *J Phys Chem C*. 2008;112(15):5825–5834.
30. Prabhu S, Poulse EK. Silver nanoparticles: mechanism of antimicrobial action, synthesis, medical applications, and toxicity effects. *Int Nano Lett*. 2012;2(1):32.
31. Wang Y, Ding X, Chen Y, et al. Antibiotic-loaded, silver core-embedded mesoporous silica nanovehicles as a synergistic antibacterial agent for the treatment of drug-resistant infections. *Biomaterials*. 2016;101:207–216.
32. Zhang L, Luo Q, Zhang F, et al. High-performance magnetic antimicrobial Janus nanorods decorated with Ag nanoparticles. *J Mater Chem*. 2012;22(45):23741–23744.
33. Lu MM, Wang QJ, Chang ZM, et al. Synergistic bactericidal activity of chlorhexidine-loaded, silver-decorated mesoporous silica nanoparticles. *Int J Nanomedicine*. 2017;12:3577–3589.
34. Du X, Li X, Xiong L, Zhang X, Kleitz F, Qiao SZ. Mesoporous silica nanoparticles with organo-bridged silsesquioxane framework as innovative platforms for bioimaging and therapeutic agent delivery. *Biomaterials*. 2016;91:90–127.
35. Yue J, Luo SZ, Lu MM, Shao D, Wang Z, Dong WF. A comparison of mesoporous silica nanoparticles and mesoporous organosilica nanoparticles as drug vehicles for cancer therapy. *Chem Biol Drug Des*. 2018;13309:1435–1444.
36. Chen SS, Xu H, Xu HJ, et al. A facile ultrasonication assisted method for Fe₃O₄@SiO₂-Ag nanospheres with excellent antibacterial activity. *Dalton Trans*. 2015;44(19):9140–9148.
37. Santoro M, Tataro AM, Mikos AG. Gelatin carriers for drug and cell delivery in tissue engineering. *J Control Release*. 2014;190:210–218.
38. Misić AM, Gardner SE, Grice EA. The wound microbiome: modern approaches to examining the role of microorganisms in impaired chronic wound healing. *Adv Wound Care*. 2014;3(7):502–510.
39. Eckhardt S, Brunetto PS, Gagnon J, Priebe M, Giese B, Fromm KM. Nanobio silver: its interactions with peptides and bacteria, and its uses in medicine. *Chem Rev*. 2013;113(7):4708–4754.
40. Fabrega J, Fawcett SR, Renshaw JC, Lead JR. Silver nanoparticle impact on bacterial growth: effect of pH, concentration, and organic matter. *Environ Sci Technol*. 2009;43(19):7285–7290.
41. Park MV, Neigh AM, Vermeulen JP, et al. The effect of particle size on the cytotoxicity, inflammation, developmental toxicity and genotoxicity of silver nanoparticles. *Biomaterials*. 2011;32(36):9810–9817.
42. dos Santos CA, Seckler MM, Ingle AP, et al. Silver nanoparticles: therapeutical uses, toxicity, and safety issues. *J Pharm Sci*. 2014;103(7):1931–1944.
43. Wilkinson LJ, White RJ, Chipman JK. Silver and nanoparticles of silver in wound dressings: a review of efficacy and safety. *J Wound Care*. 2011;20(11):543–549.
44. Du X, Kleitz F, Li X. Disulfide-bridged organosilica frameworks: designed synthesis, redox-triggered biodegradation, and nanobiomedical applications. *Adv Func Mater*. 2018;1707325.
45. Shao D, Li M, Wang Z, et al. Bioinspired diselenide-bridged mesoporous silica nanoparticles for dual-responsive protein delivery. *Adv Mater*. 2018;30:1801198.

46. Wu G, Fang YZ, Yang S, Lupton JR, Turner ND. Glutathione metabolism and its implications for health. *J Nutr*. 2004;134(3):489–492.
47. Zhao X, Lang Q, Yildirimer L, et al. Photocrosslinkable gelatin hydrogel for epidermal tissue engineering. *Adv Healthc Mater*. 2016;5(1):108–118.
48. Modaresifar K, Azizian S, Hadjizadeh A. Nano/biomimetic tissue adhesives development: from research to clinical application. *Polym Rev (Phila Pa)*. 2016;56(2):329–361.

Supplementary materials

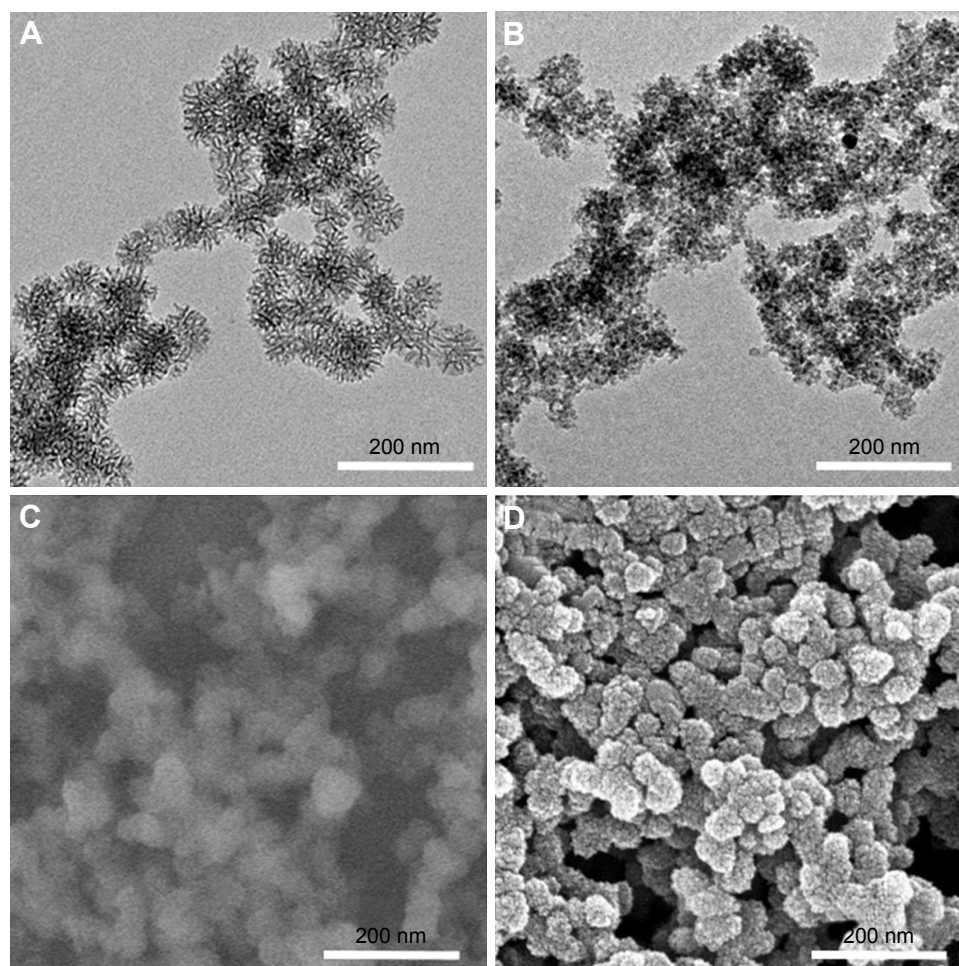


Figure S1 TEM images of (A) MSNs and (B) Ag-MSNs. SEM images of (C) MSNs and (D) Ag-MSNs.

Abbreviations: Ag-MSNs, nanosilver-decorated mesoporous silica nanoparticles; MSNs, mesoporous silica nanoparticles; SEM, scanning electron microscope; TEM, transmission electron microscope.

Table S1 Physicochemical characterization of MSNs and Ag-MSNs

Sample	MSNs	Ag-MSNs
TEM particle size (nm)	52.3±5.2	61.8±7.3
Hydrodynamic particle size (nm)	89.3±12.5	95.3±11.0
PDI	0.153	0.196
Zeta potential (mV)	-31.6±2.9	-28.5±3.4
BET surface area (m ² /g)	623.2	506.8
Total pore volume (cm ³ /g)	1.35	0.87
BJH pore size (nm)	6.6	4.1

Abbreviations: Ag-MSNs, nanosilver-decorated mesoporous silica nanoparticles; BET, Barrette–Emmett–Teller; MSNs, mesoporous silica nanoparticles; PDI, polydispersity index; TEM, transmission electron microscopy.

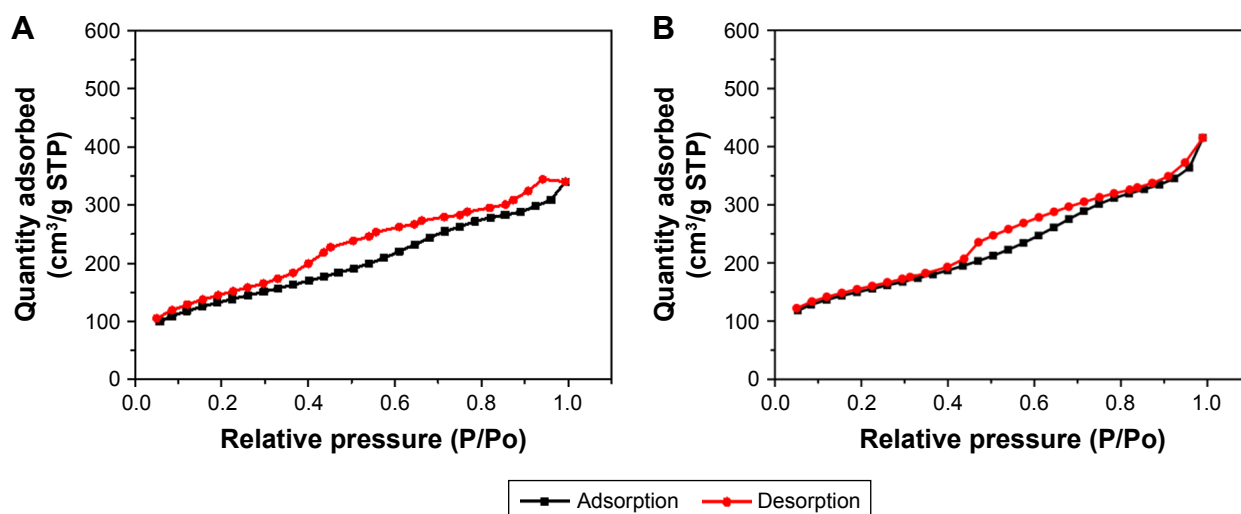


Figure S2 N_2 sorption isotherms of (A) MSNs and (B) Ag-MSNs.

Abbreviations: Ag-MSNs, nanosilver-decorated mesoporous silica nanoparticles; MSNs, mesoporous silica nanoparticles.

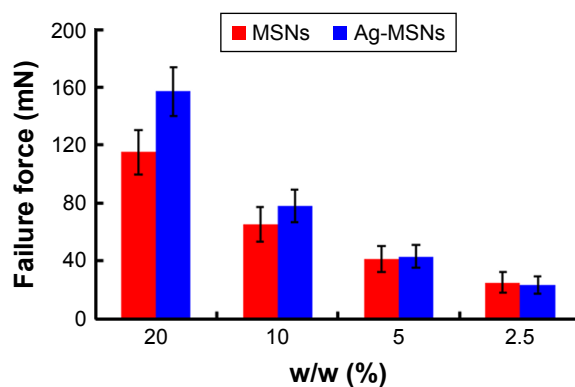


Figure S3 Failure forces of gelatin-gelatin film glued by different ratio of MSNs or Ag-MSNs.

Note: These data represent six separate experiments and are presented as the mean values \pm SD.

Abbreviations: Ag-MSNs, nanosilver-decorated mesoporous silica nanoparticles; MSNs, mesoporous silica nanoparticles.

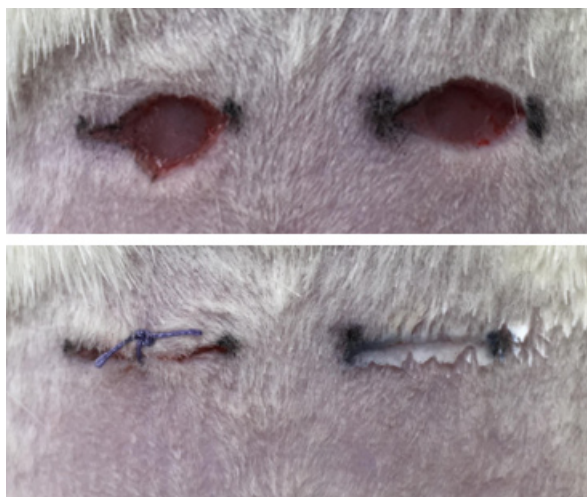


Figure S4 Representative macroscopic images of wound healing before and after treatment with ethicon suture or nano-adhesives (MSNs).

Abbreviation: MSNs, mesoporous silica nanoparticle.

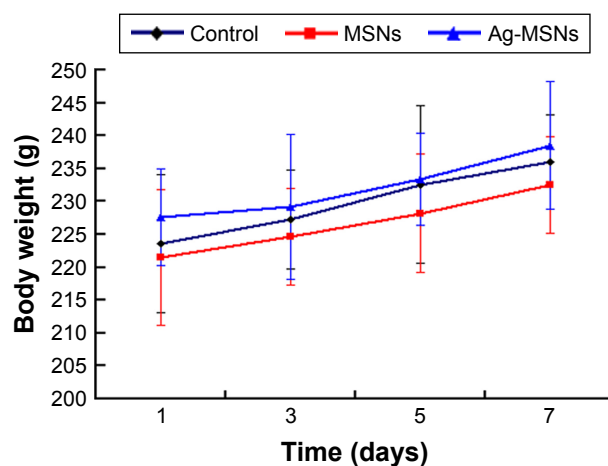


Figure S5 Body weight of rats from each group.

Note: Values are mean \pm SD, n=6.

Abbreviations: Ag-MSNs, nanosilver-decorated mesoporous silica nanoparticles; MSNs, mesoporous silica nanoparticles.

Table S2 Hematological parameters of rats treated with MSNs or Ag-MSNs

Groups	Control	MSNs	Ag-MSNs
RBC ($\times 10^{12}/L$)	7.41 \pm 1.02	7.23 \pm 0.83	7.15 \pm 0.97
WBC ($\times 10^9/L$)	10.43 \pm 3.28	10.89 \pm 3.12	10.17 \pm 2.98
PLT ($\times 10^9/L$)	702.49 \pm 286.92	789.52 \pm 312.64	756.12 \pm 258.28
Lymphocyte (%)	65.45 \pm 6.92	68.22 \pm 4.30	61.90 \pm 5.27
Monocyte (%)	7.62 \pm 0.79	7.55 \pm 0.68	7.78 \pm 0.81
MCH (pg)	15.35 \pm 0.52	15.78 \pm 0.59	16.12 \pm 0.63
MCV (fL)	46.34 \pm 3.21	45.21 \pm 3.78	45.18 \pm 2.90
HGB (g/L)	128.43 \pm 15.72	131.28 \pm 11.34	133.04 \pm 13.69

Note: Values are mean \pm SD, n=6.

Abbreviations: Ag-MSNs, nanosilver-decorated mesoporous silica nanoparticles; HGB, hemoglobin; MCH, mean corpuscular hemoglobin; MCV, mean corpuscular volume; MSNs, mesoporous silica nanoparticles; PLT, platelet; RBC, red blood cell; WBC, white blood cell.

Table S3 Biochemical parameters of rats treated with MSNs or Ag-MSNs

Groups	Control	MSNs	Ag-MSNs
AST (U/L)	211.52 \pm 23.18	203.97 \pm 21.62	218.61 \pm 18.77
ALT (U/L)	74.29 \pm 4.93	75.86 \pm 5.30	77.26 \pm 3.25
ALP (U/L)	206.49 \pm 15.90	197.52 \pm 18.38	205.36 \pm 15.11
ALB (g/L)	38.20 \pm 4.61	36.75 \pm 2.32	35.18 \pm 3.26
BUN (mmol/L)	7.21 \pm 1.89	7.16 \pm 2.57	7.38 \pm 2.87
CR (μ mol/L)	65.35 \pm 8.97	67.78 \pm 10.80	71.12 \pm 11.36
CHOL (mmol/L)	2.15 \pm 0.26	2.10 \pm 0.18	2.09 \pm 0.27
TG (mmol/L)	0.53 \pm 0.05	0.72 \pm 0.05	0.61 \pm 0.07

Note: Values are mean \pm SD, n=6.

Abbreviations: Ag-MSNs, nanosilver-decorated mesoporous silica nanoparticles; ALB, albumin; AST, aspartate aminotransferase; ALT, alanine aminotransferase; ALP, alkaline phosphatase; BUN, blood urea nitrogen; CR, serum creatinine; CHOL, cholesterol; MSNs, mesoporous silica nanoparticles; TG, triglyceride.

International Journal of Nanomedicine

Dovepress

Publish your work in this journal

The International Journal of Nanomedicine is an international, peer-reviewed journal focusing on the application of nanotechnology in diagnostics, therapeutics, and drug delivery systems throughout the biomedical field. This journal is indexed on PubMed Central, MedLine, CAS, SciSearch®, Current Contents®/Clinical Medicine,

Journal Citation Reports/Science Edition, EMBase, Scopus and the Elsevier Bibliographic databases. The manuscript management system is completely online and includes a very quick and fair peer-review system, which is all easy to use. Visit <http://www.dovepress.com/testimonials.php> to read real quotes from published authors.

Submit your manuscript here: <http://www.dovepress.com/international-journal-of-nanomedicine-journal>